Supplementary Information (SI) for Chemical Science.
This journal is © The Royal Society of Chemistry 2025

Supporting Information

Natural monosaccharide-based piezoelectric supramolecular materials for energy harvesting and information transmission

Siying Chen,[#a] Junli Yang,[#a] Shuaijie Liu,[#a] Yehong Huo,[a] Xin Cheng,[a] Lingling Li,[b] and Wei Ji*[a]

a. Key Laboratory of Biorheological Science and Technology, Ministry of Education, College of Bioengineering, Chongqing University, Chongqing 400044, China

b. Instrumental Analysis Center, Shanghai Jiao Tong University, Shanghai 200240, China

**Email: weiji@cqu.edu.cn (Wei Ji)*

[#]*S.C., J.Y. and S.L. contributed equally to this work.*

Experimental section

Materials

All solvents and chemicals were purchased from commercial suppliers and used directly without further purification.

Single crystal preparation

Monosaccharide crystals were prepared by the solvent evaporation method and heating-cooling method. The specific operation of the solvent evaporation method was as follows: we dissolved the sample in the solvent, put the solution in a 10 mL glass bottle, sealed the bottle mouth with a sealing film, and then poked five holes with a needle to evaporate slowly, gradually forming a supersaturated solution and precipitating crystals. In the heating-cooling method, the solubility of monosaccharides in the solvent was increased by heating. When the solution was cooled, the solubility decreased, the solution reached a supersaturated state, and the solute molecules spontaneously aggregated to form crystal nuclei, and eventually crystals precipitated. After multiple experimental attempts, we obtained the crystallization conditions of monosaccharides. The crystallization methods of 14 monosaccharides can be divided into three systems: aqueous crystallization system, methanol system, and mixed solvent crystallization system. In the aqueous system, α-D-Gal and β-L-Ara both precipitated crystals at a concentration of 200 mg/mL, and α-L-Rha precipitated crystals at a concentration of 100 mg/mL. In the methanol system, the following monosaccharides can be crystallized at different solution concentrations: the crystallization concentration of β-D-Fru and β-D-Psi was 150 mg/mL, the crystallization concentration of α-D-Glu, α-D-Tag and α-L-Sor was 100 mg/mL, 100 mg/mL and 10 mg/mL, respectively. In the mixed solvent system, we can further subdivide it into ethanol-water mixed system, methanol-water mixed system, and dichloromethane-organic solvent mixed system. When 10 mg/mL of β-D-All and α-L-Fuc were dissolved in ethanol: water (1:1), the solution evaporated to a supersaturated state and crystals precipitated. The concentration of α-D-Xyl sample needs to be increased to 200 mg/mL to precipitate crystals under the condition of 1:1 ethanol-water mixture. The β-D-Ara sample precipitated crystals at a concentration of 10 mg/mL methanol: water (1:1). Both α-D-Rib and β-D-dRib with a concentration of 15 mg/mL were crystallized in a mixed organic solvent of dichloromethane. α-D-Rib was crystallized using a mixed organic solvent of dichloromethane-n-propanol (7:3), while β-D-dRib was crystallized using a mixed organic solvent of dichloromethane-acetonitrile (1:1).

Powder X-Ray diffraction (PXRD)

For monosaccharide crystals with reported crystal structures, they were ground into powder and subjected to PXRD. PXRD data were collected using Cu Kα radiation (1.54056 Å, 40 mA, 40 kV). Then, the experimental data and the PXRD data of the

corresponding crystal structure were imported into the Origin software to compare the diffraction peaks and identify the crystal structure of the monosaccharide.

Single crystal X-Ray diffraction (SCXRD)

Cultivate crystal samples that meet the size requirements of single crystal diffraction and collect single crystal sample diffraction data. Firstly, the crystal was fixed to the diffractometer goniometer head and the diffraction data were collected at room temperature using a single crystal X-ray diffractometer by using DirectDrive™ rotating anode technology, which was equipped with a Helios MX multilayer monochromator (Cu Kα radiation, λ = 1.54178 Å)

Density Functional Theory (DFT) Calculations

The piezoresponse characteristics and elastic moduli of monosaccharide crystals were quantitatively assessed through periodic density functional theory (DFT) simulations implemented in the Vienna Ab Initio Simulation Package (VASP).[1] Electron exchange-correlation effects were modeled using projector-augmented wave (PAW) ·pseudopotentials combined with the Perdew-Burke-Ernzerhof (PBE) exchange-correlation functional, incorporating Grimme's D3 empirical dispersion corrections for enhanced van der Waals interactions. Structural relaxation protocols employed a 600 eV plane-wave basis set cutoff, with convergence thresholds set at 10^{-6} eV for total energy minimization and 0.01 eV/Å for residual atomic forces. Concurrently, the piezoelectric tensors (d_{ij}) were derived through self-consistent density functional perturbation theory (DFPT) calculations.

Preparation of α-D-Gal Crystals-Based Piezoelectric Nanogenerator

The preparation of piezoelectric nanogenerators required five materials: PMMA substrate, Kapton tape, copper (Cu) film, piezoelectric crystal material and PDMS.[2,3] The specific preparation process was as follows: First, a layer of Cu film (1.0 × 1.0 cm) with single-sided adhesion was laid on two PMMA substrates (1.5 × 1.5 cm) as the upper and lower electrodes. Two Cu films extended with a length of 5.0 cm and a width of 0.5 cm, respectively, for connecting the test equipment. A cubic hole (1.0 × 1.0 × 0.3 cm) was dug in the center of the PDMS membrane (2.0 × 2.0 × 0.3 cm), and then the fully ground α-D-Gal crystal powder was tightly filled into the hole. Then we used double-sided transparent tape to tightly fit the cut PDMS and copper film together, so that they were in direct contact with the piezoelectric crystal powder. Finally, Kapton tape was used to encapsulate the piezoelectric nanogenerator, ensuring that there would be no separation between the contact surface of the piezoelectric crystal powder and the copper film inside the PENG during the test.

Charge and Discharge Testing of α-D-Gal Crystals-Based Piezoelectric Nanogenerator

The alternating current generated by the α-D-Gal crystals-based PENG (4.5 × 4.5 × 0.3 cm) under external force was converted into direct current by a rectifier bridge. And the PENG was connected in series with a commercial capacitor and in parallel with a single-pole switch and LED. The charge and discharge tests were achieved by applying external force to a small motor. The motor with a speed of 150 min^{-1} applied an external force of 9.8 N to the PENG. The voltages across capacitors with five different capacitance values (0.1 μF, 0.47 μF, 1.0 μF, 3.3 μF, and 6.8 μF) were tested respectively. A digital multimeter was used to record the voltage-time response curve at room temperature throughout the experiment.

Piezoelectric Composite Film Preparation

The piezoelectric composite film consisted of three parts: a substrate layer, a conductive layer, and a piezoelectric layer.[4,5] The substrate layer was a pure PDMS film, the conductive layer was a copper foil, and the piezoelectric layer was prepared from α-D-Gal crystals powder and PDMS. The preparation of piezoelectric composite thin films included two parts: preparation of thin film precursor solution and coating thin film. (1) Preparation of precursor solution for piezoelectric composite thin film. PDMS solution preparation: PDMS and curing solution were prepared in a ratio of 10:1. Take 10 mL of PDMS solution and 1 mL of curing liquid and put them into a beaker. Stir magnetically at room temperature for 5 min to mix evenly. Ultrasonicate at room temperature for 5 min and let it stand for 10 min to eliminate bubbles. Prepare and use immediately. Preparation of PDMS/α-D-Gal crystals powder mixed solution: Grind the α-D-Gal crystals thoroughly, weigh 200 mg using an electronic balance, and put it into the prepared PDMS solution; Stir magnetically at room temperature for 20 min to eliminate bubbles. Prepare and use immediately. (2) Prepare a composite thin film by layer-by-layer coating. The prepared PDMS solution was evenly coated on a glass plate with the help of a coating rod, placed in an oven at 80°C for 8 min, and taken out to obtain a pure PDMS transparent film that was easy to remove and had stickiness. Next, an adhesive copper foil was covered on the PDMS film, and the copper foil served as a conductive electrode. Then, the prepared PDMS/α-D-Gal crystal powder mixed solution was evenly coated on a glass plate using a coating rod, placed in oven at 80°C, left to stand for 8 min, and taken out. A copper foil was attached to the piezoelectric layer film. Finally, the PDMS solution was applied on the conductive layer, and the coating rod was used to evenly coat the surface, and the solution was placed in an oven at 80°C for 8 min. The PDMS films on both sides played a role in protecting the electrodes and increasing the viscosity of the composite film. After completing the above steps, an α-D-Gal crystal piezoelectric composite film was obtained.

A list of abbreviations and corresponding full names of monosaccharide molecules.

Abbreviation	Full name
α-D-Rib	alpha-D-ribose
α-D-Xyl	alpha-D-xylose
β-D-Ara	beta-D-arabinose
β-L-Ara	beta-L-arabinose
β-D-dRib	beta-D-deoxyribose
α-D-Glu	alpha-D-glucose
α-D-Gal	alpha-D-galactose
β-D-All	beta-D-allopyranose
α-L-Rha	alpha-L-rhamnose
α-L-Fuc	alpha-L-fucose
β-D-Fru	beta-D-fructose
β-D-Psi	beta-D-psicose
α-L-Sor	alpha-L-sorbose
α-D-Tag	alpha-D-tagose

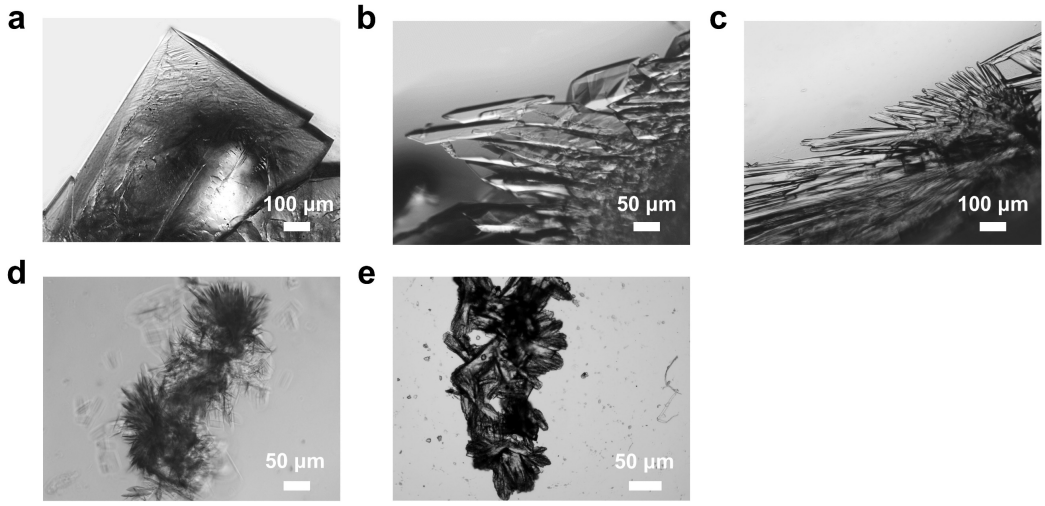

Fig. S1 Microscopy images of monosaccharide crystals. (a-e) Microscopy images of (a) β-D-Fru, (b) α-L-Fuc, (c) β-D-All, (d) β-D-dRib, and (e) α-D-Rib monosaccharide crystals.

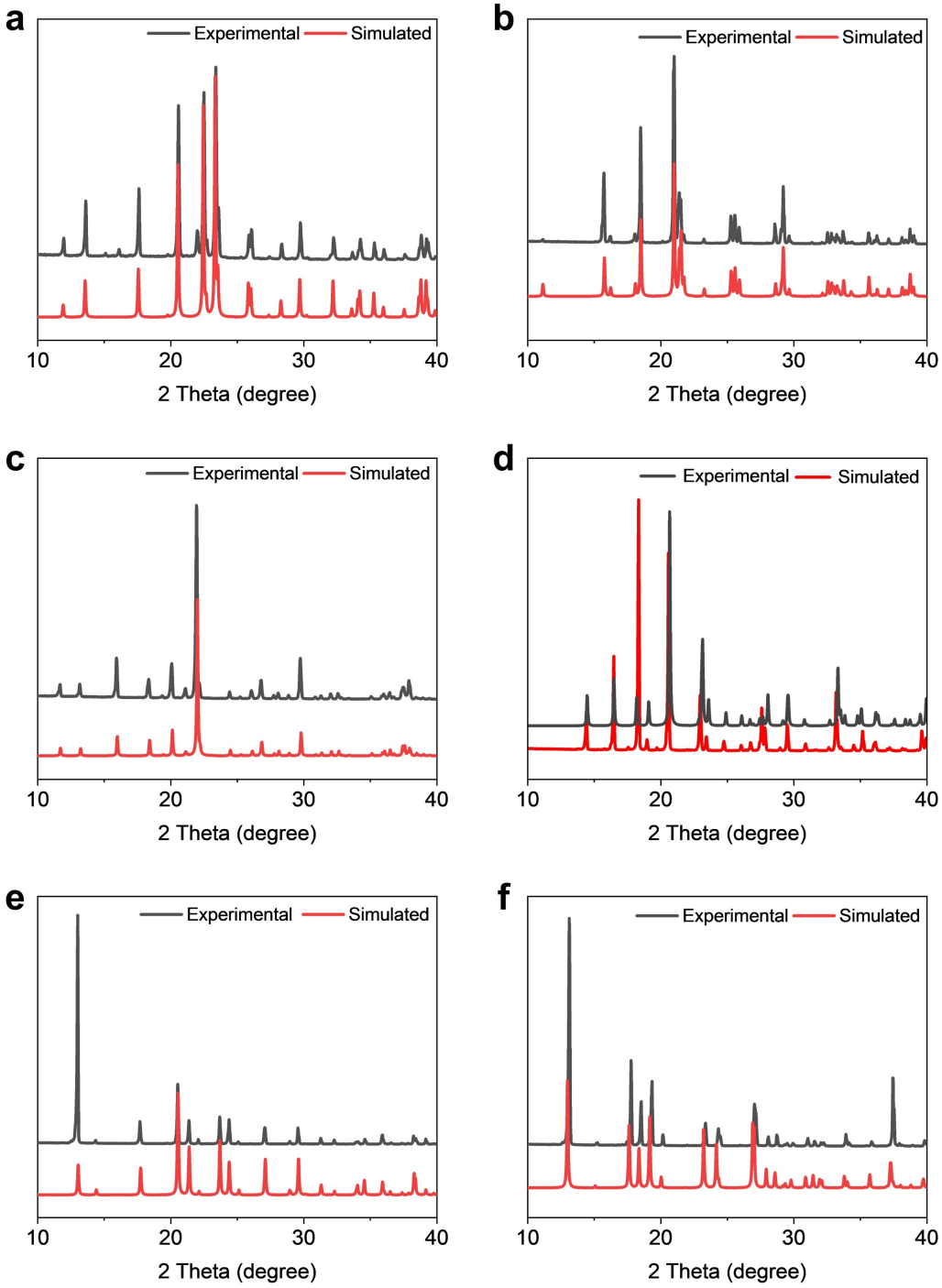

Fig. S2 Comparison of experimental PXRD data of crystals solved in this work with previously-published simulated crystal structures. (a-f) PXRD profiles of (a) β-D-All,[6] (b) α-L-Sor,[7] (c) β-D-Fru, (d) β-D-Ara,[8] (e) α-D-Gal, and (f) α-L-Rha[9] monosaccharide crystals.

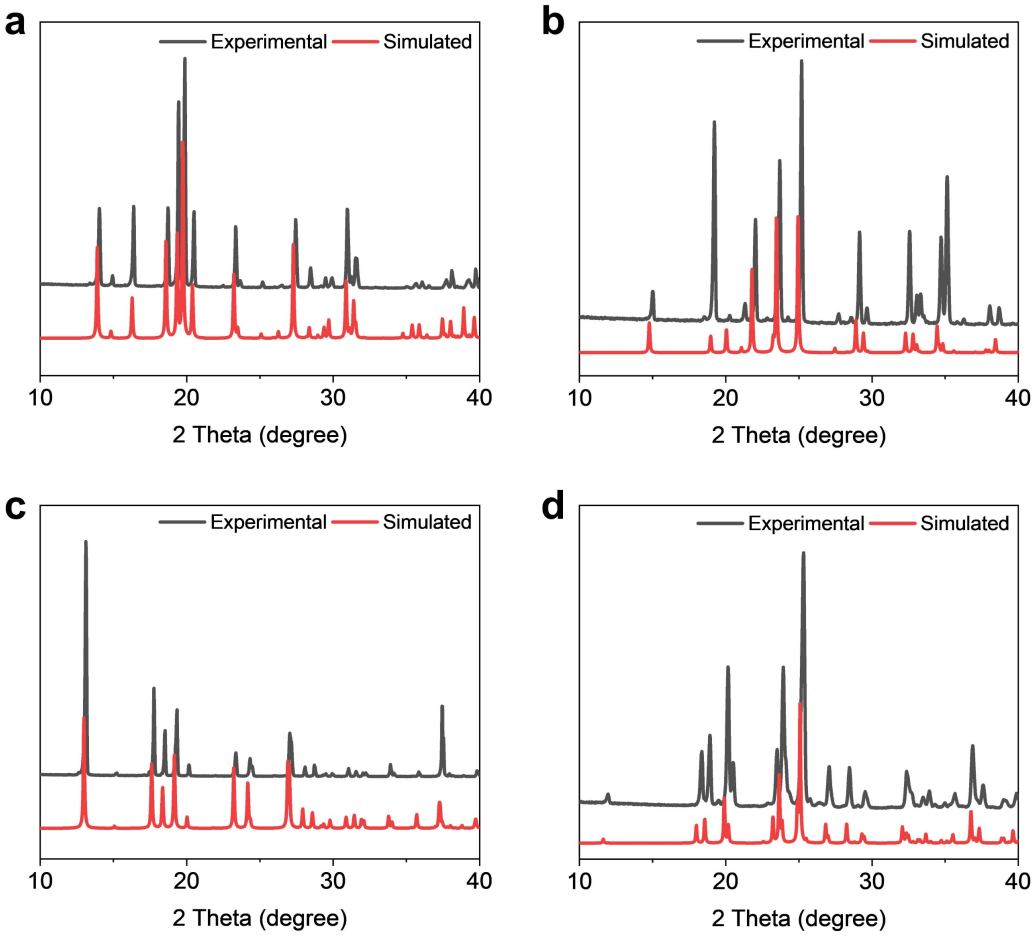

Fig. S3 Comparison of experimental PXRD data of crystals solved in this work with previously-published simulated crystal structures. (a-d) PXRD profiles of (a) α-L-Fuc,[10] (b) β-D-dRib,[11] (c) α-D-Glu,[12] and (d) α-D-Rib[13] monosaccharide crystals.

Table S1 Data collection and refinement statistics for X-ray crystallography α-D-Tag crystal.

Crystal data	α-D-Tag
Sum formula	$C_6H_{12}O_6$
Mr	180.16
Crystal system	Orthorhombic
Space group	$P2_12_12_1$
a(Å)	6.230(2)
b(Å)	6.529(2)
c(Å)	17.766(4)
α (°)	90
β (°)	90
γ (°)	90
Z	4
Mv(mm^{-1})	1.313
F000	384.0
Temperature(K)	297
Wavelength λ= (Å)	1.54178
*T*min, *T*max	0.790, 0.821
θ_{max}(°)	68.206
No. of reflections collected (unique)	10773/1291
R_{int}	0.0334
Data/restraints/parameters	1291/0/121
Goodness-of-fit on F^2	1.081
Final R_1 and wR_2 indices [$I > 2\sigma(I)$]	0.0269, 0.0715
R_1 and wR_2 indices (all data)	0.0272, 0.0718
No. CCDC	2478061

Table S2 Space groups and lattice constants of crystals formed by monosaccharides.

Name	Space groups and lattice constants
β-D-Ara	Space Group: $P2_12_12_1$ a=19.4962(3) Å α=90° b=6.44270(10) Å β=90° c=4.78330(10) Å γ=90°
β-L-Ara	Space Group: $P2_12_12_1$ a=6.535 Å α=90° b=19.467 Å β=90° c=4.841 Å γ=90°
α-D-Xyl	Space Group: $P2_12_12_1$ a=5.61070(10) Å α=90° b=9.1858(2) Å β=90° c=12.5998(3) Å γ=90°
α-D-Rib	Space Group: $P2_1$ a=4.7860(13) Å α=90° b=21.463(5) Å β=110.824(11)° c=6.4873(17) Å γ=90°
β-D-dRib	Space Group: $P2_12_12_1$ a=11.370 Å α=90° b=10.640 Å β=90° c=4.860 Å γ=90°
α-D-Glu	Space Group: $P2_12_12_1$ a=10.360 Å α=90° b=14.840 Å β=90° c=4.970 Å γ=90°
β-D-Fru	Space Group: $P2_12_12_1$ a=8.0818(4) Å α=90° b=9.1394(4) Å β=90° c=9.9546(5) Å γ=90°
α-D-Gal	Space Group: $P2_12_12_1$ a 5.939(2) Å α=90° b 7.871(2) Å β=90° c 15.800(4) Å γ=90°
β-D-All	Space Group: $P6_1$ a=16.5982 Å α=90° b=16.5982 Å β=90° c=4.8560 Å γ=119.9999°

α-L-Sor	Space Group: $P2_12_12_1$ a=6.535(4) Å α=90° b=18.069(7) Å β=90° c=6.305(4) Å γ=90°
β-D-Psi	Space Group: $P\ 2_12_12_1$ a=7.727(2) Å α=90° b=8.672(2) Å β=90° c=11.123(3) Å γ=90°
α-D-Tag	Space Group: $P\ 2_12_12_1$ a=6.230 (2) α=90° b=6.529 (2) β=90° c=17.766 (4) γ=90°
β-L-Fuc	Space Group: $P\ 2_12_12_1$ a=14.475(4) Å α=90° b=7.595(2) Å β=90° c=6.675(2) Å γ=90°
α-L-Rha	Space Group: $P\ 2_1$ a=7.901(3) Å α=90° b=7.922(3) Å β=95.52(3)° c=6.670(2) Å γ=90°

Table S3 The intermolecular hydrogen bonds and corresponding distances for β-D-Ara, α-D-Xyl, β-L-Ara, β-D-dRib. The hydrogen bonds are shown as X-H···Z and the bond length represents the distance between X and Z.

β-D-Ara	α-D-Xyl	β-L-Ara	β-D-dRib
H1-O1···O5	H4-O4···O1	H8-O1···O5	H7-O3···O1
2.758 Å	2.768 Å	2.769 Å	2.510 Å
H4-O4···O2	H5-O5···O4	H2-O4···O2	O2-H···O4
2.939 Å	2.676 Å	3.035 Å	2.871 Å
H3-O3···O2	H3-O3···O5	H10-O3···O2	O3-H2···O2
2.741 Å	2.705 Å	2.748 Å	2.891Å
H2-O2···O3	H2-O2···O3	O1-H8···O5	O3-H7···O1
2.676 Å	2.714 Å	2.769 Å	2.510 Å
O3-H3···O2	O5-H5···O4	O3-H10···O2	O3-H2···O2
2.741 Å	2.676 Å	2.748 Å	2.891 Å
O4-H4···O2	O4-H4···O1	O4-H2···O2	H-O2···O4
2.939 Å	2.768 Å	3.035 Å	2.871 Å
O2-H2···O3	O3-H3···O5	O2-H···O3	
2.676 Å	2.705 Å	2.679 Å	
	O2-H2···O3	H-O3···O2	
	2.714 Å	2.679 Å	

Table S4 The intermolecular hydrogen bonds and corresponding distances for α-D-Rib, β-D-Fru, α-D-Gal, β-D-All crystals. The hydrogen bonds are shown as X-H···Z and the bond length represents the distance between X and Z.

α-D-Rib	β-D-Fru	α-D-Gal	β-D-All
H-O11···O2A	H-O2···O5	H-O4···O2	H-O4···O1
2.798 Å	2.779 Å	2.860 Å	2.986 Å
O1-H···O12	O5-H···O2	O2-H···O4	O1-H···O4
2.824 Å	2.779 Å	2.860 Å	2.986 Å
H-O5···O3	H-O4···O2	H-O6···O1	H-O2···O2
2.700 Å	2.927 Å	2.652 Å	2.468 Å
O3-H···O5	O2-H···O4	O1-H···O6	O2-H···O2
2.782 Å	2.927 Å	2.652 Å	2.468 Å
H-O4···O13	H-O1···O2	H-O3···O4	H-O6···O6
2.820 Å	2.649 Å	2.907 Å	2.804 Å
O2A-H···O11	O2-H···O1	O4-H···O3	O6-H···O6
2.958 Å	2.649 Å	2.907 Å	2.804 Å
H-O5···O14	H-O5···O3	H-O2···O3	O4-H···O1
2.767 Å	2.808 Å	2.704 Å	2.500 Å
O13-H···O15	O3-H···O5	O3-H···O2	H-O1···O4
2.721 Å	2.808 Å	2.704 Å	2.500 Å
H-O15···O13	H-O3···O1	H-O2···O6	
2.682 Å	2.895 Å	2.765 Å	
	O1-H···O3	O6-H···O2	
	2.895 Å	2.765 Å	

Table S5 The intermolecular hydrogen bonds and corresponding distances for α-D-Glu, β-D-Psi, α-D-Tag, α-L-Fuc. The hydrogen bonds are shown as X-H···Z and the bond length represents the distance between X and Z.

α-D-Glu	β-D-Psi	α-D-Tag	α-L-Fuc
H-O1···O5	H-O3···O5	H-O6···O5	H-O3···O2
2.847 Å	2.84 Å	2.733 Å	2.84 Å
H-O3···O2	O5-H···O3	O5-H···O6	O2-H···O3
2.707 Å	2.84 Å	2.733 Å	2.84 Å
O2-H···O3	H-O6···O1	O5-H···O1	H-O2···O1
2.707 Å	2.725 Å	2.789 Å	2.742 Å
H-O4···O4	O1-H···O6	H-O2···O4	O1-H···O2
2.774 Å	2.725 Å	2.843 Å	2.742 Å
O4-H···O4	H-O1···O4	O4-H···O2	H-O1···O5
2.774 Å	2.721 Å	2.843 Å	2.756 Å
H-O2···O6	O4-H···O1	H-O2A···O4	H-O4···O3
2.775 Å	2.721 Å	2.867 Å	2.804 Å
O6-H···O2	H-O3A···O5	O4-H···O2A	O3-H···O4
2.775 Å	2.719 Å	2.867 Å	2.804 Å
H-O6···O3	H-O4···O2	H-O3···O4	
2.711 Å	2.712 Å	2.819 Å	
O3-H···O6	O2-H···O4	O4-H···O3	
2.711 Å	2.712 Å	2.819 Å	

Table S6 The intermolecular hydrogen bonds and corresponding distances for α-L-Rha and α-L-Sor crystals. The hydrogen bonds are shown as X-H···Z and the bond length represents the distance between X and Z.

α-L-Rha	α-L-Sor
H-O2···O6	H-O4···O3
2.784 Å	2.706 Å
O6-H···O2	O3-H···O4
2.784 Å	2.706 Å
H-O6···O3	H-O2···O5
3.036 Å	2.890 Å
O3-H···O6	O5-H···O2
3.036 Å	2.890 Å
H-O1···O6	H-O2A···O5
2.909 Å	2.790 Å
O6-H···O1	O5-H···O2A
2.909 Å	2.790 Å
H-O2···O1	H-O1···O3
2.715 Å	2.816 Å
O1-H···O2	O3-H···O1
2.715 Å	2.816 Å
O3-H···O5	H-O6···O4
2.809 Å	2.862 Å
H-O6···O4	
2.781 Å	
O4-H···O6	
2.781 Å	
H-O4···O6	
2.744 Å	
O6-H···O4	
2.744 Å	

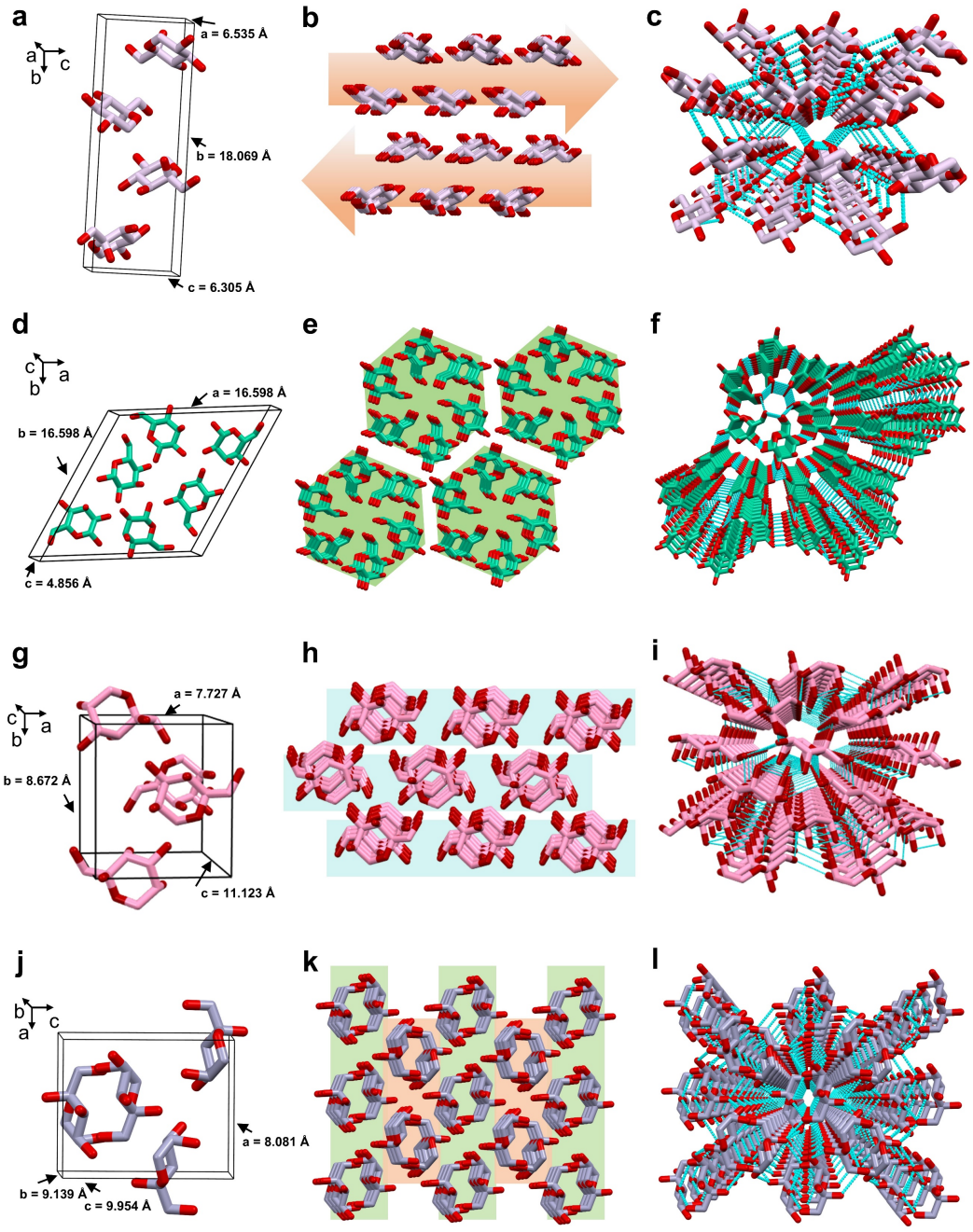

Fig. S4 Single crystal structures of α-L-Sor, β-D-All, β-D-Psi, and β-D-Fru. (a) α-L-Sor unit cell. (b) α-L-Sor slip stacking. (c) α-L-Sor crystal hydrogen bond network. (d) β-D-All unit cell. (e) β-D-All slip stacking. (f) β-D-All crystal hydrogen bond network. (g) β-D-Psi unit cell. (h) β-D-Psi slip stacking. (i) β-D-Psi crystal hydrogen bond network. (j) β-D-Fru unit cell. (k) β-D-Fru slip stacking. (l) β-D-Fru crystal hydrogen bond network. Red represents oxygen atoms, and lavender, green, pink, grey denote carbon atoms for α-L-Sor crystal, β-D-All crystal, β-D-Psi crystal, and β-D-Fru crystal, respectively.

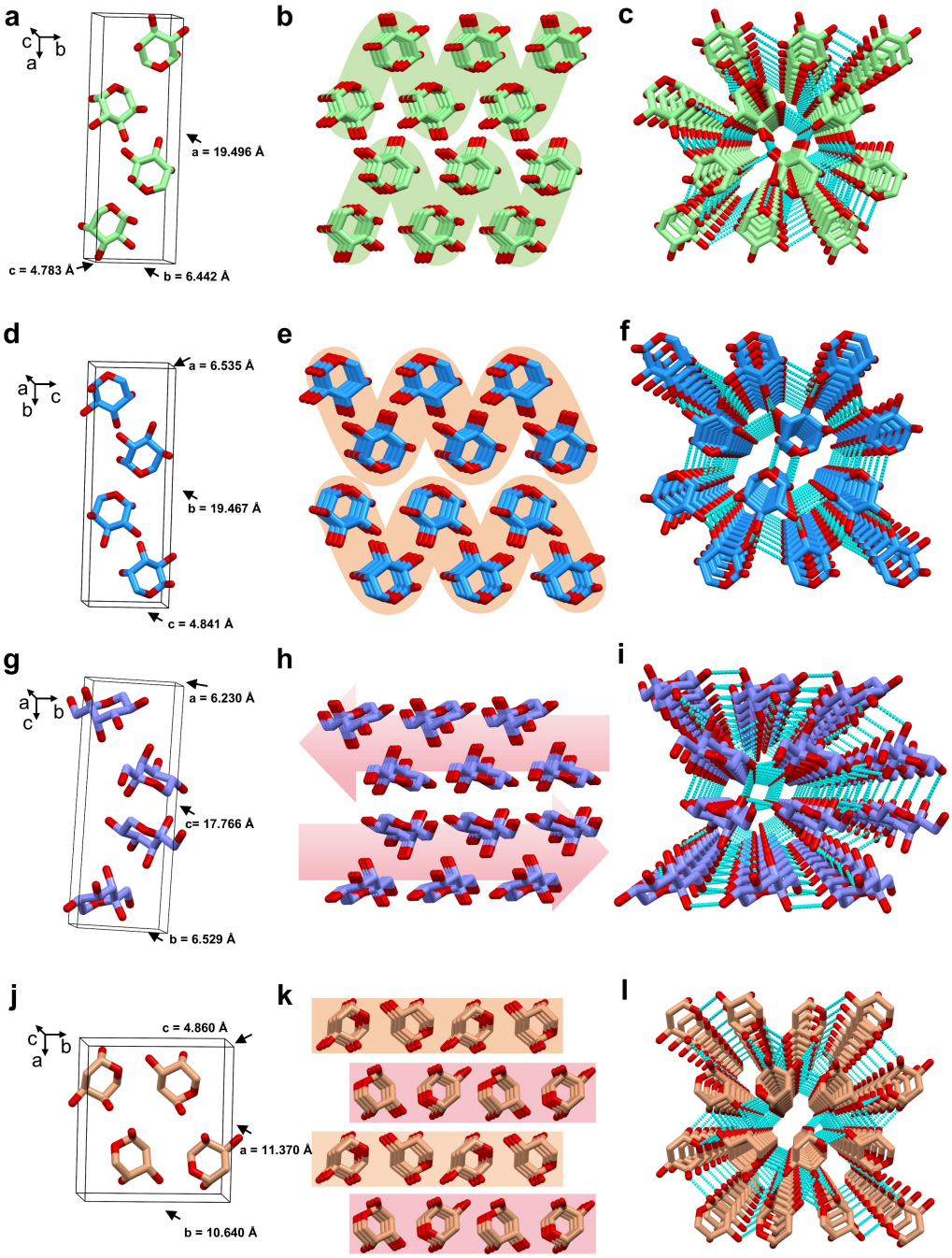

Fig. S5 Single crystal structures of β-D-Ara, β-L-Ara, α-D-Tag, and β-D-dRib. (a) β-D-Ara unit cell. (b) β-D-Ara slip stacking. (c) β-D-Ara crystal hydrogen bond network. (d) β-L-Ara unit cell. (e) β-L-Ara slip stacking. (f) β-L-Ara crystal hydrogen bond network. (g) α-D-Tag unit cell. (h) α-D-Tag slip stacking. (i) α-D-Tag crystal hydrogen bond network, (j) β-D-dRib unit cell. (k) β-D-dRib slip stacking. (l) β-D-dRib crystal hydrogen bond network. Red represents oxygen atoms, and cyan, blue, purple, brown denote carbon atoms for β-D-Ara crystal, β-L-Ara crystal, α-D-Tag crystal, and β-D-dRib crystal, respectively.

Crystal structures of the β-D-Fru, β-D-Ara, β-L-Ara, α-D-Tag, and β-D-dRib self-assemblies

β-D-Fru underwent continuous parallel extension along the *c*-axis, stabilized by hydrogen bonds H-O4···O2, O2-H···O4, H-O1···O4 and O4-H···O1 in 3D space. Ultimately, within this interconnected hydrogen-bonding network, the β-D-Fru crystals adopt a slipped stacking arrangement (Fig. S4(j-l)). β-D-Ara achieved continuous parallel extension along the *b*-axis and layer-wise stacking along the *a*- and *c*-axes through multiple hydrogen bonds. These interactions formed an intricate three-dimensional network. The resulting structure adopted a slipped stacking arrangement (Fig. S5(a-c)). β-L-Ara also crystallized in the space group $P2_12_12_1$, the four molecules in per cell unit were generated by three-fold rotation about the 2_1-screw axis (Fig. S5(d)). In the three-dimensional structure, β-L-Ara molecules exhibited continuous parallel extension along the *a*-axis through hydrogen bonds O4-H···O2 and H-O4···O2. Layer-wise and longitudinal extensions along the *c*- and *b*-axes were achieved through hydrogen bonds ranging from 2.679-2.769 Å. This intricate hydrogen-bonding network results in a slipped stacking architecture for β-L-Ara crystal (Fig. S5(e, f)). The hydrogen-bonding network of α-D-Tag crystal exhibited continuous parallel extension along the *b*-axis and layer-wise extension along the *a*-axis, while longitudinal extension along the *c*-axis occurs, which led to form a slipped arrangement (Fig. S5(g-i)). β-D-dRib displayed continuous parallel extension along the *b*-axis through hydrogen bonds O2-H···O4 and H-O2···O4. Layer-wise stacking along the *c*-axis was achieved via hydrogen bonds O3-H···O2 and H-O3···O2. While extension along the *a*-axis was stabilized by O3-H···O1 and H-O3···O1. The collective effect of intricate hydrogen-bonding network led to the formation of a slipped arrangement in β-D-dRib crystals (Fig. S5(j-l)).

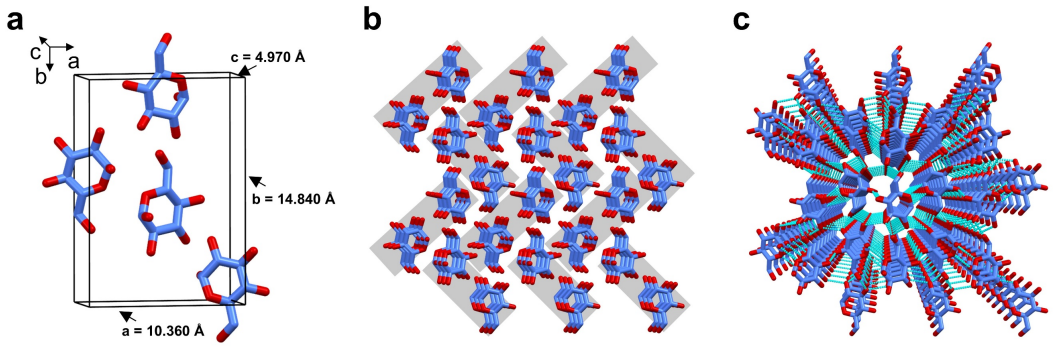

Fig. S6 Single crystal structures of α-D-Glu. (a) α-D-Glu unit cell. (b) α-D-Glu herringbone stacking. (c) α-D-Glu crystal hydrogen bond network. Red represents oxygen atoms and blue denote carbon atoms for α-D-Glu crystal.

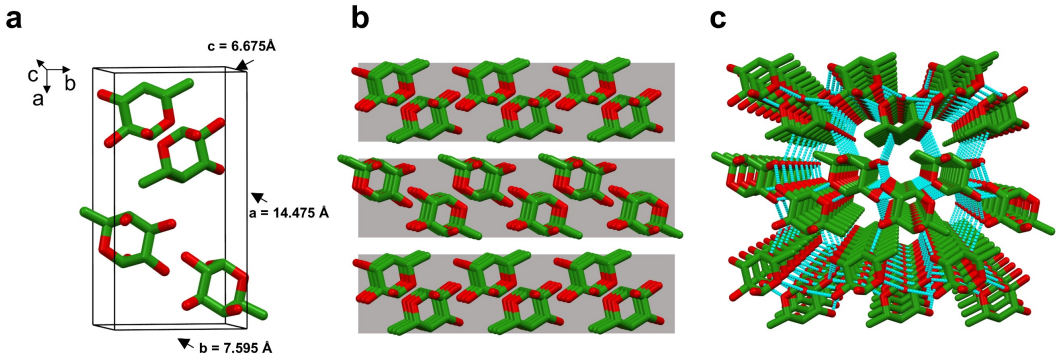

Fig. S7 Single crystal structures of α-L-Fuc. (a) α-L-Fuc unit cell. (b) α-L-Fuc parallel stacking. (c) α-L-Fuc crystal hydrogen bond network. Red represents oxygen atoms and green denote carbon atoms for α-L-Fuc crystal.

Table S7 Integration about piezoelectric coefficients of natural piezoelectric materials mentioned in the article.

Piezoelectric materials	Piezoelectric coefficient (pC/N)	Sample morphology	Measurement technique/methods	Reference
L-Valine	d_{34} = 1.8	Crystal	Calculate	14
Keratin	d_{14} = 1.8	Keratin of Horn	Quasi-static method	15
Tendon	d_{14} = 2.0	Dry samples	Quasi-static method	16
L-Proline	d_{14} = 3.35	Crystal	Calculate	17
Chitin	d_{ij} = 3.986	β-Chitin film	PFM	18
L-Threonine	d_{36} = −4.9	Crystal	Calculate	19
L-Lysine	d_{34} = 6.0	Crystal	Calculate	14
Collagen	d_{14} = 12	Collagen of rat tail tendon	PFM	20
Human Selera	d_{max} = 12	Fresh samples with anterior-posterior	PFM	21
α-D-Gal	d_{max} = 13.7	Crystal	Calculate	This work
Chitosan	d_{31} = 10	Chitosan film of Aspergillus oryzae	Piezotest	22

Table S8 Computed elastic stiffness constants of monosaccharide crystals. All values are in GPa. C_{11}, C_{22}, and C_{33} are the longitudinal stiffness constants, and C_{44}, C_{55}, and C_{66} are the shear stiffness constants.

Elastic stiffness constants	C_{11}	C_{22}	C_{33}	C_{44}	C_{55}	C_{66}
β-D-Ara	38.8	35.3	29.1	5.4	13.0	12.1
β-L-Ara	30.3	41.0	31.5	13.1	5.7	13.1
β-D-All	39.8	39.8	26.0	6.3	6.3	9.4
α-D-Xyl	22.2	23.4	46.0	10.7	8.7	8.9
α-D-Glu	42.7	61.1	21.0	6.0	8.3	16.1
α-D-Gal	21.9	34.8	32.9	11.4	9.7	14.2
β-D-Fru	26.1	26.3	39.1	9.6	17.7	9.7
β-D-Psi	38.1	24.1	8.9	14.5	5.3	11.0
α-D-Tag	46.9	46.4	26.1	11.1	7.5	19.1
α-L-Rha	25.3	31.7	47.4	10.8	6.8	8.3
α-L-Fuc	20.0	30.8	21.3	16.9	12.7	11.7
α-L-Sor	28.7	18.5	1.9	3.0	3.3	5.1
α-D-Rib	29.7	40.2	50.2	7.0	8.6	7.6
β-D-dRib	12.2	28.2	158.3	9.6	20.5	13.9

Table S9 The Young's modulus (GPa), Poisson's ratio, Bulk modulus (GPa), Shear modulus (GPa) of monosaccharide crystals.

Samples	Young's modulus (GPa)	Poisson's ratio	Bulk modulus (GPa)	Shear modulus (GPa)
α-D-Rib	25.3	0.30	20.7	9.7
β-D-Ara	25.7	0.27	18.7	10.0
β-L-Ara	26.5	0.24	17.2	10.6
β-D-All	21.0	0.34	22.4	7.8
α-D-Xyl	20.2	0.33	19.6	7.6
β-D-dRib	31.1	0.26	21.9	12.3
α-D-Glu	25.8	0.31	22.1	9.9
α-D-Gal	25.6	0.26	17.7	10.2
β-D-Fru	26.8	0.24	17.6	10.8
β-D-Psi	18.1	0.25	12.0	7.3
α-D-Tag	28.2	0.31	24.7	10.8
α-L-Rha	24.0	0.29	19.0	9.3
α-L-Fuc	21.9	0.29	17.0	8.6
α-L-Sor	6.1	0.22	4.4	2.4

Table S10 Calculated piezoelectric charge tensor components e_{ij} (in units of C/m^2), strain tensor components d_{ij} (pC/N), and voltage tensor components g_{ij} (mV m/N), of the β-D-Ara single crystal.

Charge Tensor (C/m^2)

$$\begin{pmatrix} 0 & 0 & 0 & 0.460 & 0 & 0 \\ 0 & 0 & 0 & 0 & 0.142 & 0 \\ 0 & 0 & 0 & 0 & 0 & 0.118 \end{pmatrix}$$

Strain Tensor (pC/N)

$$\begin{pmatrix} 0 & 0 & 0 & -8.5 & 0 & 0 \\ 0 & 0 & 0 & 0 & 10.9 & 0 \\ 0 & 0 & 0 & 0 & 0 & 9.7 \end{pmatrix}$$

Voltage Tensor (mV m/N)

$$\begin{pmatrix} 0 & 0 & 0 & -286 & 0 & 0 \\ 0 & 0 & 0 & 0 & 316 & 0 \\ 0 & 0 & 0 & 0 & 0 & 364 \end{pmatrix}$$

Table S11 Calculated piezoelectric charge tensor components e_{ij} (in units of C/m^2), strain tensor components d_{ij} (pC/N), and voltage tensor components g_{ij} (mV m/N), of the β-L-Ara single crystal.

Charge Tensor (C/m^2)

$$\begin{pmatrix} 0 & 0 & 0 & 0.158 & 0 & 0 \\ 0 & 0 & 0 & 0 & 0.071 & 0 \\ 0 & 0 & 0 & 0 & 0 & 0.112 \end{pmatrix}$$

Strain Tensor (pC/N)

$$\begin{pmatrix} 0 & 0 & 0 & 12.0 & 0 & 0 \\ 0 & 0 & 0 & 0 & 12.4 & 0 \\ 0 & 0 & 0 & 0 & 0 & 8.5 \end{pmatrix}$$

Voltage Tensor (mV m/N)

$$\begin{pmatrix} 0 & 0 & 0 & 349 & 0 & 0 \\ 0 & 0 & 0 & 0 & 436 & 0 \\ 0 & 0 & 0 & 0 & 0 & 321 \end{pmatrix}$$

Table S12 Calculated piezoelectric charge tensor components e_{ij} (in units of C/m^2), strain tensor components d_{ij} (pC/N), and voltage tensor components g_{ij} (mV m/N), of the α-D-Xyl single crystal.

Charge Tensor (C/m^2)

$$\begin{pmatrix} 0 & 0 & 0 & 0.019 & 0 & 0 \\ 0 & 0 & 0 & 0 & 0.064 & 0 \\ 0 & 0 & 0 & 0 & 0 & 0.032 \end{pmatrix}$$

Strain Tensor (pC/N)

$$\begin{pmatrix} 0 & 0 & 0 & 1.8 & 0 & 0 \\ 0 & 0 & 0 & 0 & 7.4 & 0 \\ 0 & 0 & 0 & 0 & 0 & 3.6 \end{pmatrix}$$

Voltage Tensor (mV m/N)

$$\begin{pmatrix} 0 & 0 & 0 & 65 & 0 & 0 \\ 0 & 0 & 0 & 0 & 258 & 0 \\ 0 & 0 & 0 & 0 & 0 & 131 \end{pmatrix}$$

Table S13 Calculated piezoelectric charge tensor components e_{ij} (in units of C/m^2), strain tensor components d_{ij} (pC/N), and voltage tensor components g_{ij} (mV m/N), of the β-D-All single crystal.

Charge Tensor (C/m^2)

$$\begin{pmatrix} 0 & 0 & 0 & 0.034 & 0.082 & 0 \\ 0 & 0 & 0 & 0.082 & -0.034 & 0 \\ 0.246 & 0.246 & 0.159 & 0 & 0 & 0 \end{pmatrix}$$

Strain Tensor (pC/N)

$$\begin{pmatrix} 0 & 0 & 0 & 5.3 & 13.0 & 0 \\ 0 & 0 & 0 & 13.0 & -5.3 & 0 \\ 3.5 & 3.5 & 2.0 & 0 & 0 & 0 \end{pmatrix}$$

Voltage Tensor (mV m/N)

$$\begin{pmatrix} 0 & 0 & 0 & 168 & 413 & 0 \\ 0 & 0 & 0 & 410 & -167 & 0 \\ 122 & 122 & 70 & 0 & 0 & 0 \end{pmatrix}$$

Table S14 Calculated piezoelectric charge tensor components e_{ij} (in units of C/m^2), strain tensor components d_{ij} (pC/N), and voltage tensor components g_{ij} (mV m/N), of the α-D-Glu single crystal.

Charge Tensor (C/m^2)

$$\begin{pmatrix} 0 & 0 & 0 & 0.015 & 0 & 0 \\ 0 & 0 & 0 & 0 & -0.050 & 0 \\ 0 & 0 & 0 & 0 & 0 & 0.080 \end{pmatrix}$$

Strain Tensor (pC/N)

$$\begin{pmatrix} 0 & 0 & 0 & 2.5 & 0 & 0 \\ 0 & 0 & 0 & 0 & -6.0 & 0 \\ 0 & 0 & 0 & 0 & 0 & 5.0 \end{pmatrix}$$

Voltage Tensor (mV m/N)

$$\begin{pmatrix} 0 & 0 & 0 & 87 & 0 & 0 \\ 0 & 0 & 0 & 0 & -198 & 0 \\ 0 & 0 & 0 & 0 & 0 & 185 \end{pmatrix}$$

Table S15 Calculated piezoelectric charge tensor components e_{ij} (in units of C/m^2), strain tensor components d_{ij} (pC/N), and voltage tensor components g_{ij} (mV m/N), of the α-D-Gal single crystal.

Charge Tensor (C/m^2)

$$\begin{pmatrix} 0 & 0 & 0 & -0.098 & 0 & 0 \\ 0 & 0 & 0 & 0 & -0.065 & 0 \\ 0 & 0 & 0 & 0 & 0 & 0.195 \end{pmatrix}$$

Strain Tensor (pC/N)

$$\begin{pmatrix} 0 & 0 & 0 & -8.6 & 0 & 0 \\ 0 & 0 & 0 & 0 & -6.7 & 0 \\ 0 & 0 & 0 & 0 & 0 & 13.7 \end{pmatrix}$$

Voltage Tensor (mV m/N)

$$\begin{pmatrix} 0 & 0 & 0 & -302 & 0 & 0 \\ 0 & 0 & 0 & 0 & -210 & 0 \\ 0 & 0 & 0 & 0 & 0 & 432 \end{pmatrix}$$

Table S16 Calculated piezoelectric charge tensor components e_{ij} (in units of C/m^2), strain tensor components d_{ij} (pC/N), and voltage tensor components g_{ij} (mV m/N), of the β-D-Psi single crystal.

Charge Tensor (C/m^2)

$$\begin{pmatrix} 0 & 0 & 0 & 0.063 & 0 & 0 \\ 0 & 0 & 0 & 0 & -0.065 & 0 \\ 0 & 0 & 0 & 0 & 0 & 0.004 \end{pmatrix}$$

Strain Tensor (pC/N)

$$\begin{pmatrix} 0 & 0 & 0 & 4.4 & 0 & 0 \\ 0 & 0 & 0 & 0 & -12.2 & 0 \\ 0 & 0 & 0 & 0 & 0 & 0.4 \end{pmatrix}$$

Voltage Tensor (mV m/N)

$$\begin{pmatrix} 0 & 0 & 0 & 127 & 0 & 0 \\ 0 & 0 & 0 & 0 & -443 & 0 \\ 0 & 0 & 0 & 0 & 0 & 16 \end{pmatrix}$$

Table S17 Calculated piezoelectric charge tensor components e_{ij} (in units of C/m^2), strain tensor components d_{ij} (pC/N), and voltage tensor components g_{ij} (mV m/N), of the α-D-Tag single crystal.

Charge Tensor (C/m^2)

$$\begin{pmatrix} 0 & 0 & 0 & 0.004 & 0 & 0 \\ 0 & 0 & 0 & 0 & 0.046 & 0 \\ 0 & 0 & 0 & 0 & 0 & 0.079 \end{pmatrix}$$

Strain Tensor (pC/N)

$$\begin{pmatrix} 0 & 0 & 0 & 0.4 & 0 & 0 \\ 0 & 0 & 0 & 0 & 6.2 & 0 \\ 0 & 0 & 0 & 0 & 0 & 4.1 \end{pmatrix}$$

Voltage Tensor (mV m/N)

$$\begin{pmatrix} 0 & 0 & 0 & 12 & 0 & 0 \\ 0 & 0 & 0 & 0 & 154 & 0 \\ 0 & 0 & 0 & 0 & 0 & 121 \end{pmatrix}$$

Table S18 Calculated piezoelectric charge tensor components e_{ij} (in units of C/m^2), strain tensor components d_{ij} (pC/N), and voltage tensor components g_{ij} (mV m/N), of the α-L-Rha single crystal.

Charge Tensor (C/m^2)

$$\begin{pmatrix} 0 & 0 & 0 & -0.014 & 0 & -0.063 \\ -0.168 & -0.057 & 0.027 & 0 & 0.070 & 0 \\ 0 & 0 & 0 & 0.025 & 0 & -0.045 \end{pmatrix}$$

Strain Tensor (pC/N)

$$\begin{pmatrix} 0 & 0 & 0 & -1.0 & 0 & -7.6 \\ -7.4 & -0.2 & 2.0 & 0 & 10.2 & 0 \\ 0 & 0 & 0 & 2.5 & 0 & -5.6 \end{pmatrix}$$

Voltage Tensor (mV m/N)

$$\begin{pmatrix} 0 & 0 & 0 & -36 & 0 & -274 \\ -236 & -6 & 64 & 0 & 325 & 0 \\ 0 & 0 & 0 & 91 & 0 & -205 \end{pmatrix}$$

Table S19 Calculated piezoelectric charge tensor components e_{ij} (in units of C/m^2), strain tensor components d_{ij} (pC/N), and voltage tensor components g_{ij} (mV m/N), of the α-L-Fuc single crystal.

Charge Tensor (C/m^2)

$$\begin{pmatrix} 0 & 0 & 0 & -0.153 & 0 & 0 \\ 0 & 0 & 0 & 0 & -0.001 & 0 \\ 0 & 0 & 0 & 0 & 0 & -0.089 \end{pmatrix}$$

Strain Tensor (pC/N)

$$\begin{pmatrix} 0 & 0 & 0 & -9.1 & 0 & 0 \\ 0 & 0 & 0 & 0 & -0.1 & 0 \\ 0 & 0 & 0 & 0 & 0 & -7.6 \end{pmatrix}$$

Voltage Tensor (mV m/N)

$$\begin{pmatrix} 0 & 0 & 0 & -316 & 0 & 0 \\ 0 & 0 & 0 & 0 & -3 & 0 \\ 0 & 0 & 0 & 0 & 0 & -274 \end{pmatrix}$$

Table S20 Calculated piezoelectric charge tensor components e_{ij} (in units of C/m^2), strain tensor components d_{ij} (pC/N), and voltage tensor components g_{ij} (mV m/N), of the α-L-Sor single crystal.

Charge Tensor (C/m^2)

$$\begin{pmatrix} 0 & 0 & 0 & -0.030 & 0 & 0 \\ 0 & 0 & 0 & 0 & 0.041 & 0 \\ 0 & 0 & 0 & 0 & 0 & -0.038 \end{pmatrix}$$

Strain Tensor (pC/N)

$$\begin{pmatrix} 0 & 0 & 0 & -9.9 & 0 & 0 \\ 0 & 0 & 0 & 0 & 12.4 & 0 \\ 0 & 0 & 0 & 0 & 0 & -7.5 \end{pmatrix}$$

Voltage Tensor (mV m/N)

$$\begin{pmatrix} 0 & 0 & 0 & -288 & 0 & 0 \\ 0 & 0 & 0 & 0 & 304 & 0 \\ 0 & 0 & 0 & 0 & 0 & -274 \end{pmatrix}$$

Table S21 Calculated piezoelectric charge tensor components e_{ij} (in units of C/m^2), strain tensor components d_{ij} (pC/N), and voltage tensor components g_{ij} (mV m/N), of the α-D-Rib single crystal.

Charge Tensor (C/m^2)

$$\begin{pmatrix} 0 & 0 & 0 & 0.036 & 0 & 0.038 \\ 0.060 & -0.001 & 0.041 & 0 & -0.036 & 0 \\ 0 & 0 & 0 & 0.061 & 0 & 0.010 \end{pmatrix}$$

Strain Tensor (pC/N)

$$\begin{pmatrix} 0 & 0 & 0 & 5.2 & 0 & 5.0 \\ 2.1 & -0.8 & 0.4 & 0 & -4.2 & 0 \\ 0 & 0 & 0 & 8.6 & 0 & 1.4 \end{pmatrix}$$

Voltage Tensor (mV m/N)

$$\begin{pmatrix} 0 & 0 & 0 & 196 & 0 & 186 \\ 72 & -27 & 14 & 0 & -144 & 0 \\ 0 & 0 & 0 & 273 & 0 & 44 \end{pmatrix}$$

Table S22 Calculated piezoelectric charge tensor components e_{ij} (in units of C/m^2), strain tensor components d_{ij} (pC/N), and voltage tensor components g_{ij} (mV m/N), of the β-D-dRib single crystal.

Charge Tensor (C/m^2)

$$\begin{pmatrix} 0 & 0 & 0 & -0.012 & 0 & 0 \\ 0 & 0 & 0 & 0 & -0.131 & 0 \\ 0 & 0 & 0 & 0 & 0 & -0.020 \end{pmatrix}$$

Strain Tensor (pC/N)

$$\begin{pmatrix} 0 & 0 & 0 & 1.2 & 0 & 0 \\ 0 & 0 & 0 & 0 & -6.4 & 0 \\ 0 & 0 & 0 & 0 & 0 & 1.4 \end{pmatrix}$$

Voltage Tensor (mV m/N)

$$\begin{pmatrix} 0 & 0 & 0 & 37 & 0 & 0 \\ 0 & 0 & 0 & 0 & -209 & 0 \\ 0 & 0 & 0 & 0 & 0 & 46 \end{pmatrix}$$

Table S23 Calculated piezoelectric charge tensor components e_{ij} (in units of C/m^2), strain tensor components d_{ij} (pC/N), and voltage tensor components g_{ij} (mV m/N), of the β-D-Fru single crystal.

Charge Tensor (C/m^2)

$$\begin{pmatrix} 0 & 0 & 0 & -0.033 & 0 & 0 \\ 0 & 0 & 0 & 0 & -0.015 & 0 \\ 0 & 0 & 0 & 0 & 0 & -0.078 \end{pmatrix}$$

Strain Tensor (pC/N)

$$\begin{pmatrix} 0 & 0 & 0 & -3.4 & 0 & 0 \\ 0 & 0 & 0 & 0 & -0.8 & 0 \\ 0 & 0 & 0 & 0 & 0 & -8.1 \end{pmatrix}$$

Voltage Tensor (mV m/N)

$$\begin{pmatrix} 0 & 0 & 0 & -107 & 0 & 0 \\ 0 & 0 & 0 & 0 & -26 & 0 \\ 0 & 0 & 0 & 0 & 0 & -264 \end{pmatrix}$$

Table S24 Computed relative permittivity (ε_i) and dielectric constants (ε_r) of the monosaccharide crystals. All values are unitless.

Dielectric constant	ε_1	ε_2	ε_3	ε_r
α-D-Rib	3.04	3.29	3.56	3.30
β-D-Ara	3.36	3.90	3.01	3.42
β-L-Ara	3.89	3.29	2.99	3.39
β-D-All	3.58	3.58	3.25	3.47
α-D-Xyl	3.12	3.27	3.11	3.17
α-D-dRib	3.66	3.46	3.46	3.53
α-D-Glu	3.23	3.43	3.06	3.24
α-D-Gal	3.22	3.60	3.58	3.47
β-D-Fru	3.60	3.49	3.47	3.52
β-D-Psi	3.9	3.11	2.81	3.27
α-D-Tag	3.83	4.56	3.84	4.08
α-L-Rha	3.13	3.55	3.09	3.26
α-L-Fuc	3.25	3.33	3.14	3.24
α-L-Sor	3.88	4.61	3.09	3.89

Table S25 Predicted molecular and crystal dipole moments of monosaccharides.

Sample	Molecular dipole moments (Debye, D)	Crystal dipole moments (Debye, D)
α-D-Rib	2.5	0.5
β-D-Ara	2.3	3.5
β-L-Ara	3.0	2.2
β-D-All	5.8	7.3
α-D-Xyl	1.8	0.5
β-D-dRib	1.8	0.2
α-D-Glu	2.5	0.9
α-D-Gal	4.7	7.4
β-D-Fru	2.6	1.1
β-D-Psi	3.4	4.4
α-D-Tag	2.6	1.5
α-L-Rha	2.4	3.2
α-L-Fuc	1.9	0.4
α-L-Sor	2.5	0.4

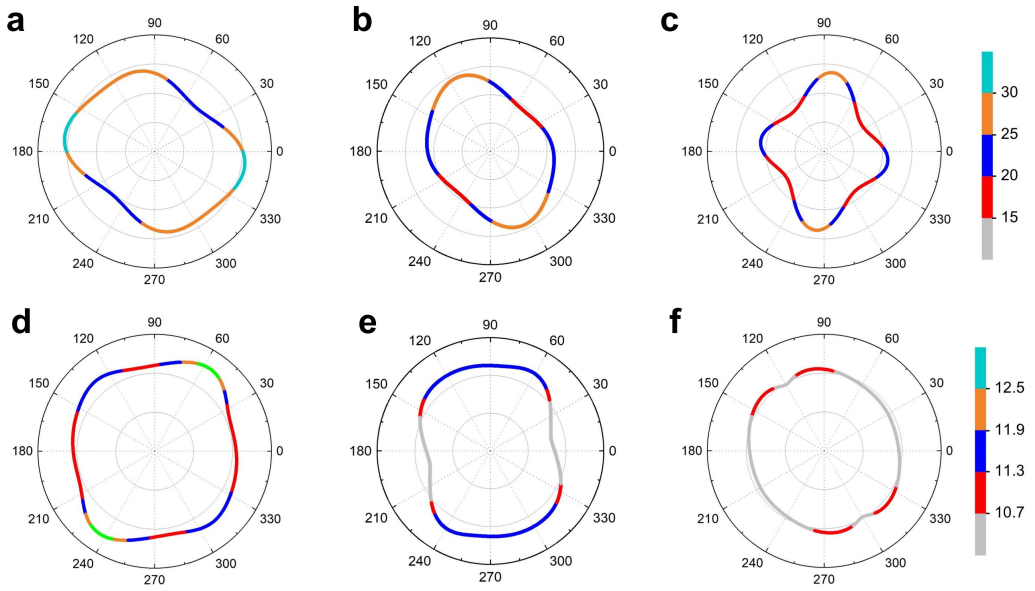

Fig. S8 Study on piezoelectric properties of monosaccharide crystals. The angle dependence relations of the (a-c) Young's modulus (GPa), and (d-f) shear modulus (GPa) of (a, d) α-D-Gal, (b, e) α-L-Rha, and (c, f) α-D-Xyl crystals.

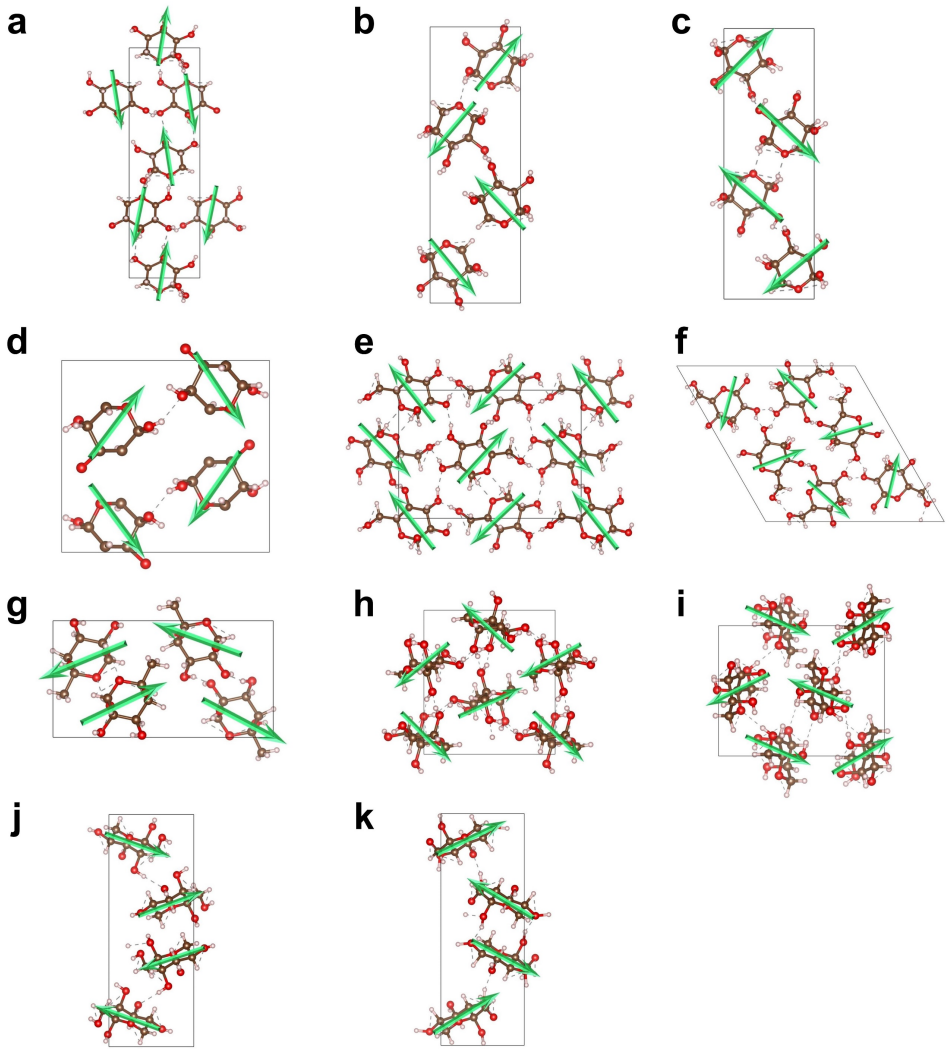

Fig. S9 Dipole moment arrangement model of monosaccharides crystals. (a) α-D-Rib, (b) β-D-Ara, (c) β-L-Ara, (d) β-D-dRib, (e) α-D-Glu, (f) β-D-All, (g) α-L-Fuc, (h) β-D-Fru, (i) β-D-Psi, (j) α-D-Tag, and (k) α-L-Sor crystals.

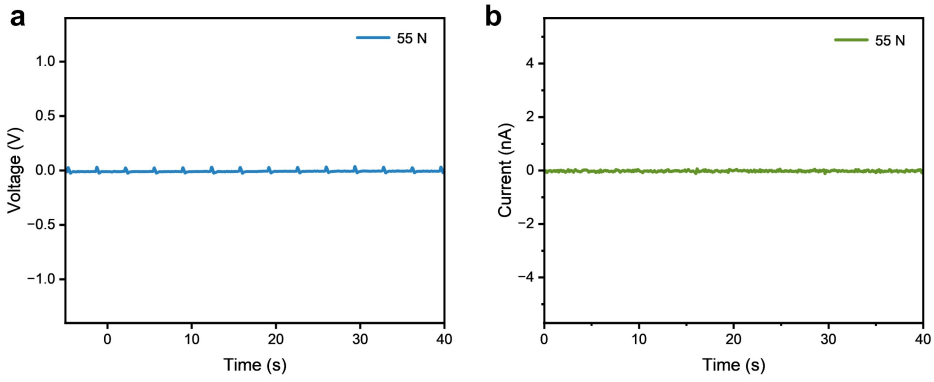

Fig. S10 (a) Output voltage and (b) output current generated by the PENG without α-D-Gal crystals under mechanical force of 55 N.

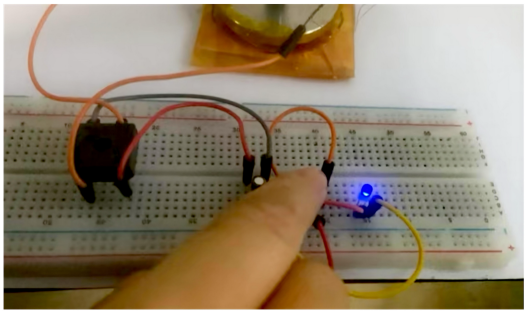

Fig. S11 Characteristics of the output performance of the α-D-Gal crystals-based PENG. The piezoelectric nanogenerator can light an LED by charging the 0.1 μF capacitor for 1min.

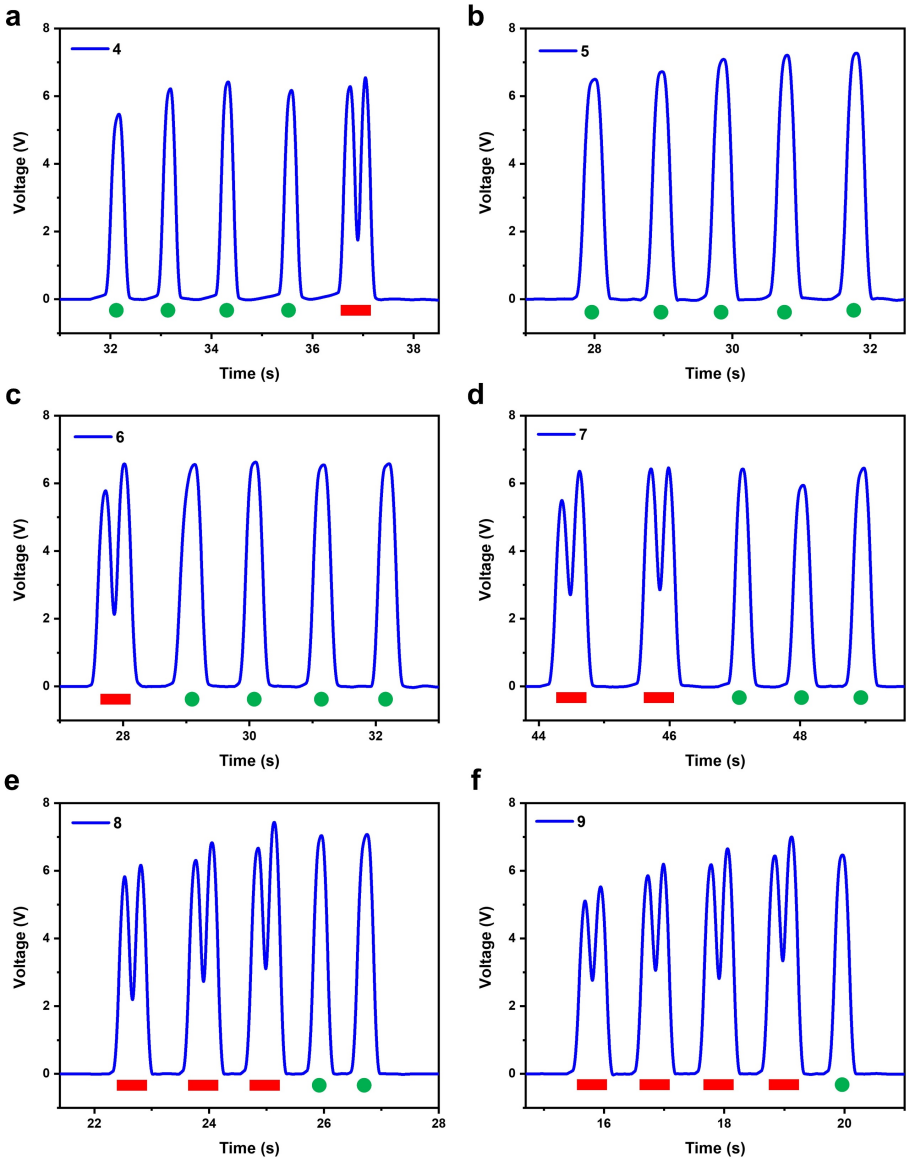

Fig. S12 Application of α-D-Gal crystals-based piezoelectric film. Morse code. (a) "4", (b) "5", (c) "6", (d) "7", (e) "8", and (f) "9" was generated by piezoelectric composite film.

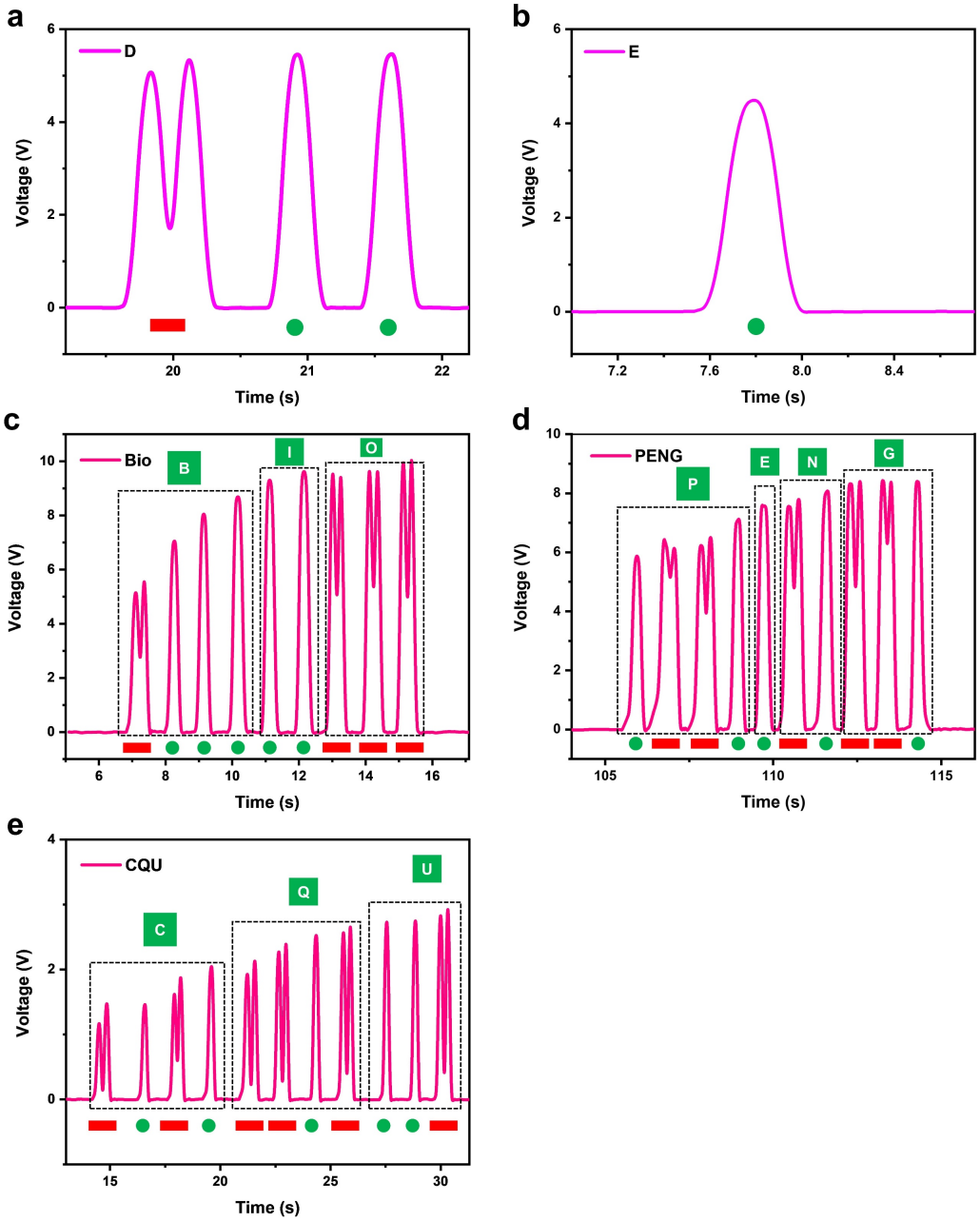

Fig. S13 Application of α-D-Gal crystals-based piezoelectric film. Morse code (a) "D", (b) "E", (c) "Bio", (d) "PENG", and (e) "CQU" was generated by piezoelectric composite film.

References

1 J. Hafner, *Comput. Phys. Commun.*, 2007, **177**, 6-13.

2 W. Ji, B. Xue, Z. A. Arnon, H. Yuan, S. Bera, Q. Li, D. Zaguri, N. P. Reynolds, H. Li, Y. Chen, S. Gilead, S. Rencus-Lazar, J. B. Li, R. S. Yang, Y. Cao and E. Gazit, *ACS Nano*, 2019, **13**, 14477-14485.

3 S. Azimi, A. Golabchi, A. Nekookar, S. Rabbani, M. H. Amiri, K. Asadi and M. M. Abolhasani, *Nano Energy*, 2021, **83**, 105781.

4 C. X. Luo, S. H. Hu, M. J. Xia, P. W. Li, J. Hu, G. Li, H. B. Jiang and W. D. Zhang, *Energy Technol.*, 2018, **6**, 922-927.

5 I. S. S. Vamsi, N. K. Das and S. Badhulika, *Mater. Sci. Semicond. Process*, 2024, **169**, 107945.

6 P. A. Bonnet, J. van de Streek, A. V. Trask, W. D. S. Motherwell and W. Jones, *Crystengcomm*, 2004, **6**, 535-539.

7 S. H. Kim and R. D. Rosenstein, *Acta Crystallographica*, 1967, **22**, 648.

8 B. Tyson, C. M. Pask, N. George and E. Simone, *Cryst. Growth Des.*, 2022, **22**, 1371-1383.

9 S. Takagi and G. Jeffrey, *Structural Sci.*, 1978, **34**, 2551-2555.

10 F. Longchambon, J. Ohannessian, D. t. Avenel and A. Neuman, *Structural Sci.*, 1975, **31**, 2623-2627.

11 S. Furberg, *Acta Chem. Scand.*, 1960, **14**, 9.

12 G. M. Brown and H. A. Levy, *Science*, 1965, **147**, 1038.

13 D. Sisak, L. B. McCusker, G. Zandomeneghi, B. H. Meier, D. Bläser, R. Boese, W. B. Schweizer, R. Gilmour and J. D. Dunitz, *Angew. Chem. Int. Edit.*, 2010, **49**, 4503-4505.

14 Y. H. Wang, S. J. Liu, L. L. Li, H. Li, Y. Y. Yin, S. Rencus-Lazar, S. Guerin, W. E. Ouyang, D. Thompson, R. S. Yang, K. Y. Cai, E. Gazit and W. Ji, *J. Am. Chem. Soc.*, 2023, **145**, 15331-15342.

15 E. Kar, M. Barman, S. Das, A. Das, P. Datta, S. Mukherjee, M. Tavakoli, N. Mukherjee and N. Bose, *Sustain. Energ. Fuels*, 2021, **5**, 1857-1866.

16 D. Kim, S. A. Han, J. H. Kim, J. H. Lee, S. W. Kim and S. W. Lee, *Adv. Mater.*, 2020, **32**, 1906989.

17 S. Guerin, T. A. M. Syed and D. Thompson, *Nanoscale*, 2018, **10**, 9653-9663.

18 K. Kim, M. Ha, B. Choi, S. H. Joo, H. S. Kang, J. H. Park, B. Gu, C. Park, C. Park, J. Kim, S. K. Kwak, H. Ko, J. Jin and S. J. Kang, *Nano Energy*, 2018, **48**, 275-283.

19 S. Guerin, S. A. M. Tofail and D. Thompson, *Cryst. Growth Des.*, 2018, **18**, 4844-4848.

20 D. Denning, J. I. Kilpatrick, E. Fukada, N. Zhang, S. Habelitz, A. Fertala, M. D. Gilchrist, Y. Zhang, S. A. M. Tofail and B. J. Rodriguez, *ACS Biomat. Sci. Eng.*, 2017, **3**, 929-935.
21 S. Ghosh, B. Z. Mei, V. Lubkin, J. I. Scheinbeim, B. A. Newman, P. Kramer, G. Bennett and N. Feit, *J. Biomed. Mater. Res.*, 1998, **39**, 453-457.
22 A. Amran, F. B. Ahmad, M. H. M. Akmal, A. A. M. Ralib and M. I. Bin Suhaimi, *Mater. Today Commun.*, 2021, **29**, 102919.